


Daily rhythms drive dynamism in sleep, oscillations and interneuron firing, while excitatory firing remains stable across 24 h

Nicolette Ognjanovski^{1,2}  | David S. Kim¹ | Emma Charlett-Green² | Ethan Goldiez¹ | Sofie van Koppen² | Sara J. Aton³ | Brendon O. Watson¹

¹Department of Psychiatry, University of Michigan, Ann Arbor, Michigan, USA

²Cell and Chemical Biology, Leiden University Medical Center, Leiden, Netherlands

³Department of Molecular, Cellular, and Developmental Biology, University of Michigan, Ann Arbor, Michigan, USA

Correspondence

Nicolette Ognjanovski, Department of Psychiatry, University of Michigan Medicine, Ann Arbor, MI 48109, USA.
Email: nnognjan@umich.edu

Funding information

J.B. and M.K. Pritzker Family Foundation; National Institute of Health Sciences, Grant/Award Number: MH107662; Marie Curie Horizons 2020 Leading Fellowship, Grant/Award Number: 707404; A. Alfred Taubman Medical Research Institute; Eisenberg Depression Center; University of Michigan Neuroscience Scholars; Michigan Medicine Sleep Disorders Center; Gilmore Sleep Fellowship

Edited by: Hanspeter Landolt

Abstract

The adaptation to the daily 24-h light–dark cycle is ubiquitous across animal species and is crucial for maintaining fitness. This free-running cycle occurs innately within multiple bodily systems, such as endogenous circadian rhythms in clock-gene expression and synaptic plasticity. These phenomena are well studied; however, it is unknown if and how the 24-h clock affects electrophysiologic network function in vivo. The hippocampus is a region of interest for long timescale (>8 h) studies because it is critical for cognitive function and exhibits time-of-day effects in learning. We recorded single cell spiking activity and local field potentials (LFPs) in mouse hippocampus across the 24-h (12:12-h light/dark) cycle to quantify how electrophysiological network function is modulated across the 24-h day. We found that while inhibitory population firing rates and LFP oscillations exhibit modulation across the day, average excitatory population firing is static. This excitatory stability, despite inhibitory dynamism, may enable consistent around-the-clock function of neural circuits.

KEYWORDS

circadian, electrophysiology, network, rhythm, spiking

Abbreviations: CA1, cornu ammonis 1; DB, Davies–Bouldin; DG, dentate gyrus; EBS, electrophysiologic background signature; EEG, electroencephalographic; EIB, electronic interface board; EMG, electromyographic; LFP, local field potential; NREM, non-rapid eye movement; PCA, principal component analysis; pE, putative excitatory; pI, putative inhibitory; PSD, power spectral density; PV, parvalbumin; REM, rapid eye movement; SCN, suprachiasmatic nucleus; SFC, spike-field coherence; SPWRs, sharp-wave ripples; SWS, slow-wave sleep; ZT, zeitgeber time.

This is an open access article under the terms of the [Creative Commons Attribution-NonCommercial-NoDerivs](https://creativecommons.org/licenses/by-nc-nd/4.0/) License, which permits use and distribution in any medium, provided the original work is properly cited, the use is non-commercial and no modifications or adaptations are made.

© 2024 The Author(s). *European Journal of Neuroscience* published by Federation of European Neuroscience Societies and John Wiley & Sons Ltd.

1 | INTRODUCTION

A variety of brain-based functions, including activity level, feeding, neurotransmitter-specific transmission, and sleep–wake cycling, occur on timescales embedded in the 24-h (circadian) 12 h:12 h light:dark cycle, which dictates healthy brain baseline (Eckel-Mahan, 2012; Jilg et al., 2010). Extensive work both in vivo and ex vivo has demonstrated daily rhythmicity in the firing of neurons of the brain's central pacemaker, the suprachiasmatic nucleus (SCN). The SCN is also the 'master clock', as it electrically and molecularly synchronizes the brain as a whole through 24-h molecular rhythms of clock-associated proteins and transcripts (Brown & Piggins, 2009; Ramkisoensing & Meijer, 2015; Schaap et al., 2003).

Indeed, many 24-h studies in non-SCN brain regions have focused on molecular or synaptic measures, and the changes are often reported through metabolomic and transcriptomic analysis across the day. However, no such 'omic' exists for electrical output across 24-h. Despite action potential generation ('firing' or 'spiking') playing a pivotal role in neural function—ultimately driving behaviour and perception—hourly reports across 24-h are not as frequent. Some high-quality reports do indeed exist (Brecht et al., 2003; Delgado, 1952; Houben et al., 2009; Mariscal et al., 2023; Miyawaki & Diba, 2016; Thomas et al., 2020; van Oosterhout et al., 2012), but these have focused most frequently on local field potential (LFP) rather than spiking data, or analyses have centred frequently on non-circadian questions. One possible reason for the relatively few papers in this space is the historical difficulty in recording and especially spike-sorting long-duration recordings, but this barrier has been significantly reduced with improved computer capacities and spike-sorting algorithms. Relatedly, most in vivo electrophysiologic studies are typically analysed over much shorter (<8 h) durations, which does not lend itself to 24-h contextual interpretation. Additionally, in vitro preparations, even when carried out over circadian timescales, lack some degree of interpretability given the removal of behaviour, modulatory drive, and other impacts on in vivo brain physiology (Bridi et al., 2020; Paul et al., 2020). On the other hand, in vivo freely behaving recordings and analyses are often temporally locked to experimenter-defined tasks, manipulations, or units of perception (i.e., place or stimulus) or focus on brain states such as sleep/wake (Skilling et al., 2021; Watson et al., 2016). Such approaches have been crucial in helping us understand many aspects of neuroscience but do not lend themselves to changes in ongoing background network status that might occur across the day.

We know that an individual will react differentially to the same stimulus at different times of day (Russell & Lightman, 2019); therefore, given that network spiking controls behaviour, we hypothesize that neural networks adopt different configurations at different times of day. A region of particular interest is the hippocampus because it is critical for cognition and is an information integration centre for both social and spatial contexts (Maurer & Nadel, 2021; Oliva et al., 2020; Terranova et al., 2022) and shows circadian rhythmicity in both clock-gene expression and synaptic plasticity (Eckel-Mahan, 2012; Frank, 2021; Rawashdeh et al., 2018).

We quantify here for the first time what we call the 'electrophysiologic background signature' (EBS) in the hippocampus over 24-h light/dark periods. We define EBS as the ongoing spiking and oscillatory activities of circuits that are not task-specific but rather are a 'network tone' or a continuum of hourly snapshots, analogous to a proteomic profile, that may mediate differential behavioural reactivity. Here, we set out to define daily rhythms in the hippocampus by recording for 24-h periods from mouse hippocampal networks using tetrodes. We find striking contrasts between excitatory and inhibitory neural populations around the clock and consider the presented EBS metrics a necessary baseline to note when conducting further long-term studies.

2 | MATERIALS AND METHODS

2.1 | Animal use

The results here were originally recorded as part of data sets for Ognjanovski et al., 2014 and Ognjanovski et al., 2017 (all recordings used here were performed prior to any behavioural interventions or learning), as well as discarded baseline recordings of animals that did not complete behavioural training (as in the reported publications) and were thus discarded from those analyses. Revisiting old data with a new perspective, 'circadian' or 'time-of-day', as presented here versus 'response to learning', allowed us to collect recordings from the 10 animals without the use of new animals.

2.2 | Mouse handling

All animal husbandry and surgical/experimental procedures were approved by the University of Michigan Institutional Animal Care and Use Committee (PRO00003931—Sleep and Brain Plasticity in the Mouse to SJA). Male C57BL/6J mice ($n = 10$;

IMSR_JAX:000664, Jackson) were individually housed in standard caging with environmental enrichment (nesting material, tunnels, treats) throughout all pre- and post-operative procedures. Environmental light was maintained on a 12:12 light:dark cycle (lights on at 8:00 AM, zeitgeber time [ZT] 0) with food and water available ad libitum consistently before and during recordings.

2.3 | Micro-drive fabrication

Tetrodes were created using a 40 cm long piece of insulated nickel-chromium wire (20 μm diameter, California Fine Wire) cut out from a roll and folded twice, creating a bundle of four wires. Wires were twisted using a tetrode twister (OpenEphys) with 80 \times clockwise spins and 30 \times counterclockwise spins. A heat gun was used to melt the polyamide insulation to the bundle into a single tetrode. The tetrode was threaded through a 1 mm-wide custom-bored screw attached to a custom-modified 32-channel electronic interface board (EIB-36-PTB-Narrow, Neuralynx) with two of each micro-electrode from the tetrode bundle coupled to one channel with connections secured using gold pins. In total, seven tetrodes were affixed to the board in addition to two reference wires. The EIB and wires were covered with Diafil (Diadent) to prevent damage. The tip of the tetrodes was bound, cut at a 45 $^\circ$ angle, and impedance was measured using Nano Z (Neuralynx) hardware/software. Tetrodes were electroplated with Sifco 5355 gold plating solution (Neuralynx) with a target of 350 k Ω as previously described (Ognjanovski et al., 2014, 2017).

2.4 | Surgical procedures

At age 15–23 weeks, mice were implanted with custom-built, drivable head stages with two bundles of tetrodes (3–4 tetrodes each) threaded through two ferrules spaced 4 mm apart under isofluroane anesthesia as previously published (Ognjanovski et al., 2014, 2017). Each tetrode bundle was implanted within the dorsal part of hippocampal region cornu ammonis 1 (CA1) (relative to Bregma: 1.75–2.75 mm posterior, 1.5–2.5 mm lateral and 1.0 mm ventral) in both right and left hemispheres. In addition, two screws were attached above the cerebellum in both the right and left cerebellum, to which we attached an electroencephalographic (EEG) and reference wire, respectively. We also placed electromyographic (EMG) wires in the nuchal muscle for additional characterization of sleep states and movement artifacts.

2.5 | Single-cell recording

Mice were prepared for chronic recording 1 week after implantation surgery as previously described (Ognjanovski et al., 2014, 2017). Signals from each electrode were split and differentially filtered to obtain spike data (200 Hz–8 kHz) and LFP/EEG data (0–200 Hz) at each recording site. Data were amplified at 20 \times , digitized, further digitally amplified a t 40 \times and recorded using OmniplexTM hardware and software (Plexon Inc.; Dallas, TX). Following acclimation for 3 days, electrode bundles were lowered into the hippocampus until stable recording signals were achieved. Referencing of all tetrode bundles was done to an internal reference for the Headstage and EIB interface (EIB-36 Neuralynx and RHD-32ch Headstage Intan #C3314). When the internal reference was unavailable, we used a tetrode channel empty of neural signal (for example, on an unused bundle) to set as an internal signal reference for the other channels. We waited for waveforms to be continuously present on the same channels for at least 24 h, after which a continuous 24-h recording period began coincident with lights-on (ZT0) for use in the analysis presented here.

Single neuron data were discriminated offline using standard principal component analysis (PCA, Offline Sorter; Plexon). Tetrode data was discriminated using a stereotrode model (Plexon Offline sorter) to decrease noise across channels. Individual neurons were discriminated based on spike waveform, relative spike amplitude on the two stereotrode recording wires, relative positioning of spike waveform clusters in 3D principal component space and neuronal subclass (i.e., pE-cells, excitatory; pI-cells, inhibitory). Neurons with spike half-width less or equal to 0.5 ms were classified as pI-cells. Spike cluster discrimination in principal component space was verified using MANOVA p values <0.05 and Davies–Bouldin (DB) indices ≥ 0.25 , as previously described (Ognjanovski et al., 2017).

2.6 | Cosinor analysis

We iteratively fitted multiple sine waves to each of the time series (with different period lengths) to quantify which sinusoid had the best fit using the Cosinor Analysis toolbox (<https://www.mathworks.com/matlabcentral/fileexchange/20329-cosinor-analysis>, MATLAB Central File Exchange, retrieved 19 August 2021). Cosinor analysis uses the least squares method to fit a sine wave to a time series, as outlined in Nelson et al. (1979). For our analysis, we used the following inputs: t - time series time

points (1 h bins 24 repetitions), y - value of series at time t , which is raw power spectral density (PSD) for each hour for each neuron independently, w - cycle length, defined by the user based on prior knowledge of time series (here using the basis of the 24-h cycle of 1 day), and alpha-type I error used for confidence interval calculations (0.05, as indicated in the literature). Analysis then yielded a degree of fit for each sinusoid with cells that fit the 24-h cycle and sub-harmonics (6 and 12 Hz) characterized as 'rhythmic'. All cells were characterized, and a percent of total for each cell type was calculated (p-I and p-E).

2.7 | Sleep state and interval analysis

Intrahippocampal LFP and nuchal EMG signals were used to manually categorize each 10-s interval of recording as NREM, REM or wake across 24-h using custom spectrograph presentation software as previously described (Ognjanovski et al., 2014). The percentage of time spent in NREM, REM, and wake was calculated for each mouse on an hour per hour basis with the total time (s) of each state (NREM, REM, wake) divided by the 3600 s bin size. Noise artifacts were excluded, therefore some hour bins had less than 3600 s in the denominator. This ratio was then multiplied by 100 to display the percentage of total time for each hour. Bouts were measured as the length in seconds of each uninterrupted occupation of state >10 s and averaged within each hour for each state. For sleep state interval analysis, the function 'MakeSleepStates' was used to create three vectors categorized into sleep state bouts (duration), inter-sleep state duration, and the proportion of the time spent in the sleep. These states were compared with the inter-sleep state duration that followed for interval windows of wake, NREM and REM.

2.8 | Firing rate analysis

State-specific analysis of cell firing was first assessed by measuring cell spike frequency in sleep states within 1-h time bins. For each reliably discriminated neuron (pE-cells, $n = 108$; pI-cells, $n = 21$ across 10 animals), mean firing frequency was calculated within each behavioural state (REM, slow-wave sleep [SWS] and wakefulness) across 24 h for each neuron. The rate was calculated as spikes per second within that state within that hour. Data is shown as average frequency across each 1-h bin for the duration of the recording.

2.9 | LFP analyses

Recordings were low-pass filtered (0–1000 Hz) on each tetrode channel as previously described in Ognjanovski et al., 2014, 2017. Raw PSD from 0 to 100 Hz was generated via Fourier techniques every 0.1 s to create a spectrogram. For all animals and recordings, these bins begin at zeitgeber time zero and are tiled without overlap thereafter for 24 h. This analysis was calculated on each channel (~ 30 /animal), where spike data was stably recorded throughout the experiment.

For frequency band analysis, the following bands were analysed: delta (0.5–3.9 Hz) during NREM and theta (4–10 Hz) for REM and wake. To quantify band power, we averaged the power for each frequency within the respective band in 1-min bins within each hour and state. The hour bins were locked to the zeitgeber time 0 and minute bins tiled 1–60 within each hour. Within a given hour, not all minutes will show each state, so when state power is presented for a given hour of the day, we only include minutes that include that particular state and extract band power within those minutes. If any hour has zero occupancy in a given state for a given animal, the LFPs from that animal for that hour were not used. This gave us power per hour in a given state in a single animal. Then this power was averaged on an hourly bin-wise basis for the power values obtained during periods of, for example, REM sleep over the entire recording is then used as reference, and we normalized our hourly average by dividing each hour by this value. So for at any ZT time (1-h) time bin. it is divided by that animal's average daily power across all 24 hours for that frequency band (say REM theta). These hourly normalized values were averaged to present full-dataset findings across animals.

LFP band power within each state was used to calculate frequency band power vs. time using Neuroexplorer software (NexTechnologies, Boulder, CO). Ripples were additionally quantified within NREM sleep in 1-h windows using previously described methods (Ognjanovski et al., 2017). Briefly, LFPs were bandpass filtered (150–250 Hz), and ripple events were automatically detected using a threshold of six or more consecutive cycles of an oscillation with a voltage ± 2.5 S.D. from baseline signal mean. Ripples were detected independently on each LFP channel for each animal using the same (baseline) voltage threshold. Each ripple detected was denoted as an event with a start and stop time. Ripple power (PSD) was then quantified within these time events for each hour and normalized as LFPs above (divided each hour by daily average). All reliable LFP channels were treated equally, independent of animal recording, as long as they were active during the same state during the recording hour.

2.10 | Spike-field coherence

Spike-field coherence (SFC) relies on the function made by Timothy Olsen (2022): ‘Spike-signal coherence’ (<https://www.mathworks.com/matlabcentral/fileexchange/72755-spike-signal-coherence>), MATLAB Central File Exchange. Retrieved 10 June 2022. We began by loading the LFP, spike trains and sleep states by running the script SpikeFieldCoherence.m. LFP is filtered to the desired band with the Signal Processing Toolbox ‘bandpass’ function. Then the function MakeParentSleepSpkandLFP.m creates a cell array that holds the coherence scores from 0 to 1.0 (1 being most coherent and 0 being least coherent) for each frequency per spike train (neuron). This iterated over a range of frequencies 1–500 Hz (via ‘Olsen’s function’). Per sleep state bout, the median coherence value is taken and stored. Each of these values is plotted over time over the midpoint of their bouts to create a ‘coherence curve’. A filtered (8-point, moving mean) coherence curve was used for cross-neuron averaging. Each spike train is analysed to produce a coherence curve, but spike trains with frequencies <0.1 Hz in a sleep state bout for a given hour are not used, and no coherence metric is output for that channel. The spike trains that failed to return valid values for over 95% of assessed frequency bands were excluded from further quantification and visualization.

2.11 | Statistical analysis

Statistical analysis was performed on data obtained by individual electrodes ($n = 16$ –28 channels per animal). This includes both individual cell spike rates or SFC and individual LFPs. These values were averaged across 10 sets of observations (each animal). To determine the effect of time, a one-way ANOVA was conducted across the 24 one-hour bins (each bin a group with multiple samples per group coming from $n = 10$ animals). Shapiro–Wilk tests for normality and Brown–Forsythe equal variance showed the validity of using ANOVA. If circadian effects were observed, differences between hours were statistically analysed using pairwise multiple comparison procedures (Holm–Sidak, Tukey’s, Dunn’s method, as mentioned in individual figure legends). Calculations were performed with Graphpad Prism (v.9, Graphpad Software Inc., San Diego, CA, USA) and Sigma plot (v.14.5, Systat Software, Palo Alto, CA, USA). Further support was provided by CSCAR statistical services at the University of Michigan (Ann Arbor, USA). Measures with p values < 0.05 are defined as significant relationships. Detailed statistics for Figures 2 and 3 are shown in Tables S1–S3.

3 | RESULTS

Using tetrodes, we recorded spikes and LFP from hippocampal CA1 of C57BL/6 mice (Jackson Labs, $n = 10$), unperturbed, in their home cages for 24-h under 12 h:12 h light/dark conditions (Figure 1a). No animals had any ongoing or prior experimenter-induced learning or experiences. We were able to verify significant circadian periodicity in actigraphy (Figure 1b) across all animals.

3.1 | Daily electrophysiologic rhythm of the hippocampus shows ultradian inhibitory rhythmicity but stable excitatory activity

Individual cell activity within and across animals appeared to show variation across the circadian day (Figure 1c,d). This pattern was consistent when averaging between or within animals (Figure 1e). To provide further resolution on this and quantify effects, we separated spiking activity from two types of neurons based on waveform shape: putative excitatory (pE-, $n = 108$) and putative inhibitory (pI-, $n = 21$) cells (Figure 1f,g) (Hu et al., 2014; Ognjanovski et al., 2017). Firing rates of pE- and pI-cells were quantified across 24 h using 1-h bins starting at lights-on (Figure 1h, ZTX = X hours after lights-on). Based on prior work showing behavioural, synaptic, neurochemical and molecular dynamism over the day, we expected to see changes in spiking over the day. We found that pI-cells do indeed show rhythmic daily activity (Figure 1h, top). At ZT9 and ZT15–17, we observe troughs that had significantly lower firing rates than the daily average ($p < 0.05$, hour-by-hour statistics described in Section 2). We also observe that before lights-off at ZT12, pI-cell firing frequency begins to increase, implying a biological rhythm not purely driven by environmental light changes.

Surprisingly, in contrast to pI-cell dynamics, per-hour pE-cell firing rates showed no significant deviation from the full-day mean (Figure 1h, bottom). Further supporting this difference between pE and pI dynamics, only 18.5% of pE-cells ($n = 20$) show statistically significantly rhythmic activity when fitted within 24-h cycles via cosinor analysis, while 90.5% of pI-cells ($n = 19$) show rhythmic activity (Figure 1i). Thus, the daily rhythmicity in CA1 is specific to pI-cells but not pE-cells.

3.2 | Stable pE-cell firing persists even when controlling for sleep states

We next determined whether the observed firing rate changes might be mediated by the varying sleep/

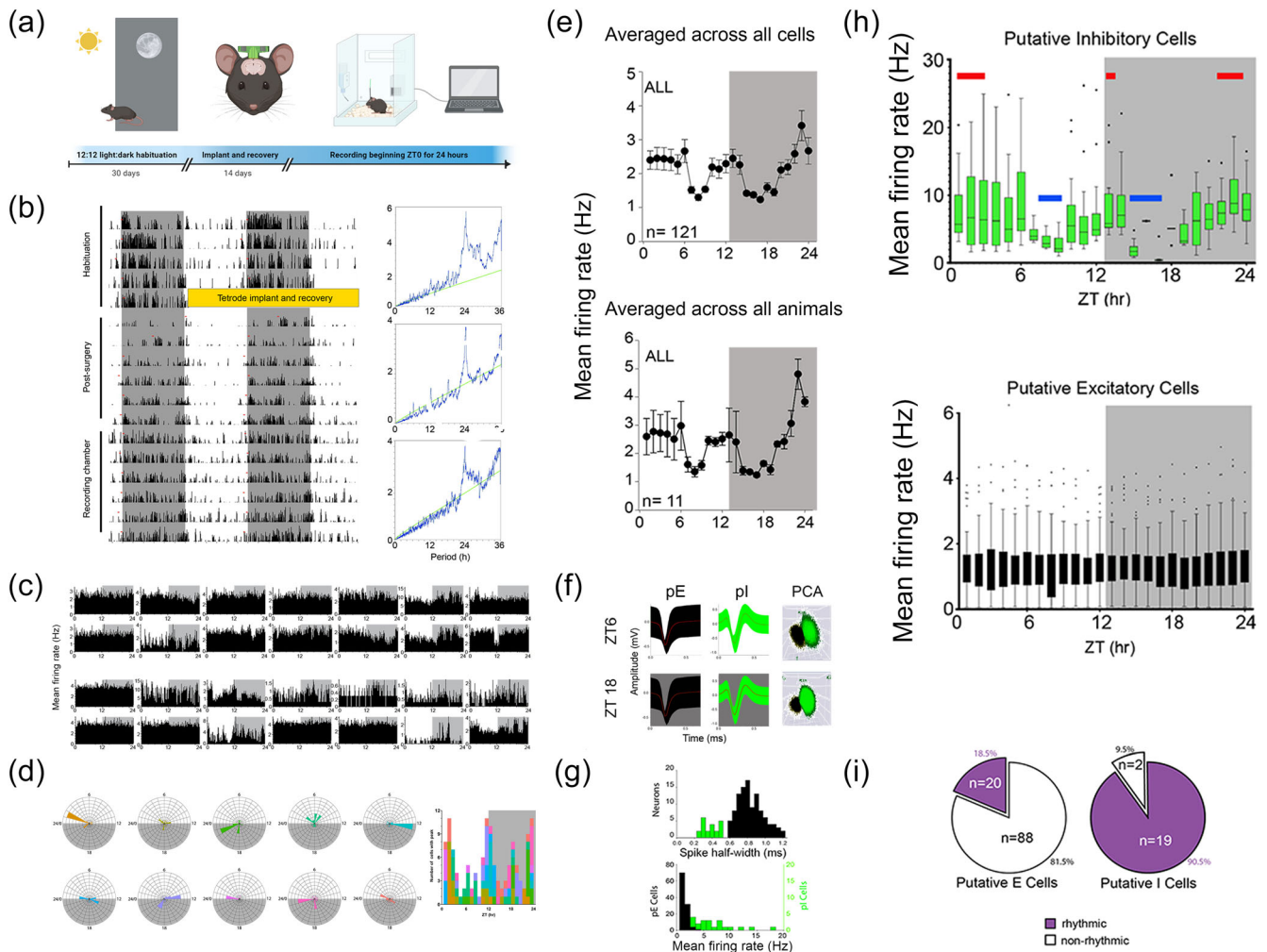


FIGURE 1 Daily rhythm of hippocampal neuronal firing shows ultradian modulation of inhibitory activity but stable excitatory activity (a) Schematic of experimental setup including habituation, implantation and recording. (b) Locomotor behaviour before implantation, following tetrode craniotomy, recovery and during the recording period: double plotted actigraphy for representative mouse for 30 days. Plotted with 12:12 light: dark cycle with greyed bars indicating dark phase. Periodograms to the right show the daily mouse behaviour period of ~ 24 -h. (c) Example firing rate plots of all neurons recorded from two individual animals across 24-h of recording showing variation in individual raster activity. (d) Left: radial plots of the peak firing times of each of the cells for individual animals (each animal is a radial plot and colour). Each tick out from the centre on the radial plot is five neurons. Right: quantification of timings of peak firing for all individual cells ($n = 129$) (e) Mean firing rate per hour shown averaged across all cells (top)—treating all animals as equal—and then summing firing of all cells within an animal and averaging across animals (bottom, $n = 10$) (f) Distinguishing units into putative excitatory versus inhibitory subtypes. Recording from one tetrode bundle implanted in dorsal cornu ammonis 1 (CA1). Left: two resulting spike waveforms from the same tetrode at mid-light and mid-dark phase (ZT6 and ZT18, respectively). Right: principal component analysis (PCA) profile from the same tetrode, showing location of each action potential in space. Putative excitatory (pE)-cell action potentials are shown in black and putative inhibitory (pI)-cell action potentials are shown in green for circadian time shown at left. (g) After selecting for stable units, data across all 24-h of recording for each cell type (pI-cells, green and pE-cells, black) was characterized on two additional metrics: distribution of spike half-width across cells (top) and overall firing rate distribution of pI-cells ($n = 21$) and p-I cells ($n = 108$). (h) Average firing rate per hour for 24-h recordings starting at ZT0 for pI-cells (green, top). Red bars indicate peaks above the 24-h mean based on pairwise multiple comparisons (ZT1–3, ZT12–13 and ZT21–23). Blue bars indicate significant troughs (ZT8–9 and ZT15–17). Graph is box and whisker with outliers shown as black dots. Background shading indicates the 12:12 light/dark schedule: grey for dark. Average firing rate per hour for pE-cells (black) did not reveal any hours significantly differing from the 24-h mean. (i) Pie chart indicating the number of arrhythmic (white) and rhythmic (purple) cells for each of pE-cells (18.5%) and pI-cells (90.4%) as assessed by cosinor analysis (see Section 2). Statistical analysis with Fisher's exact test.

wake-state occupancies across the day-night. We classified sleep states from behavioural EMG and LFP (Figure 2a) and measured firing rates only within epochs of wake, rapid eye movement (REM), and non-rapid eye movement (NREM) sleep for each hour (Figure 2b). First, the tendencies of each neuron to fire at their peak frequency at a given time of day do show variance (Figure 2b, black bars), but they do not clearly correspond with sleep state occupancy (Figure 2b, coloured

dots). Sleep state bout duration and inter-bout intervals were also analysed and shown in Figure 2c (see also Figure S1).

Within each sleep state, the activity of pI-cells continued to exhibit rhythmicity across the day (Figure 2d–f), qualitatively similar to the overall pattern without state separation. We again observed two troughs: late-day (ZT9) and early-night (ZT17) and two peaks in early (ZT14) and late (ZT24) night across all states ($p < 0.001$

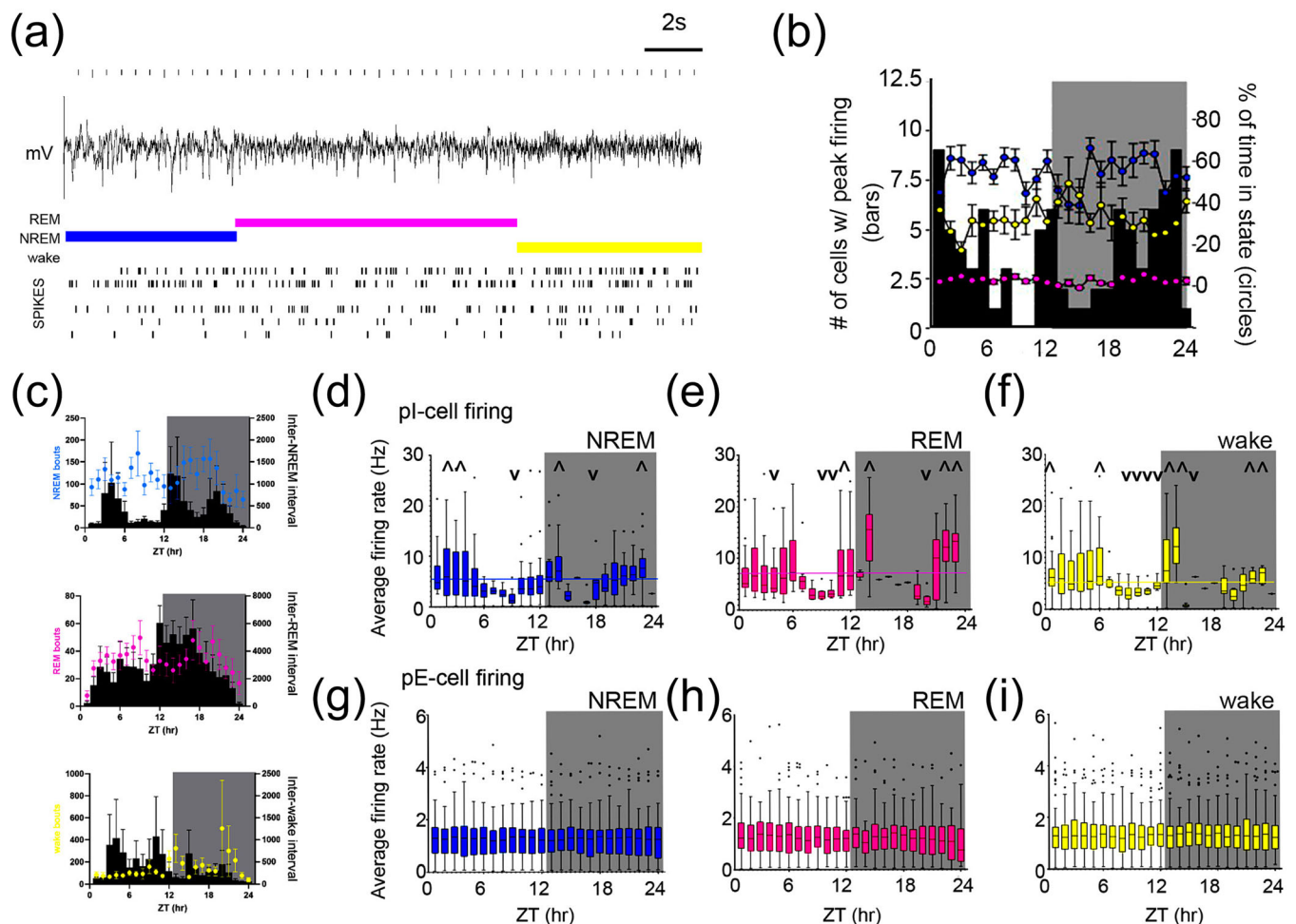


FIGURE 2 Stable excitatory signalling persists independent of sleep state, while p-I firing dynamics anticipate light change (a) Sleep was characterized using combined behavioural and local field potential (LFP) data. Example spike raster for one animal shown for 40 s. Coloured bars above traces indicate assigned state: wake (yellow), non-rapid eye movement (NREM) (blue) and rapid eye movement (REM) (pink). (b) Sleep state does not dictate timing of peak firing rate for all neurons. Connected coloured dots on each plot are the percent occupancy (right axis) of each state. Black bars: the number of total neurons (out of $n = 129$) having peak firing rate in that hour (left axis). (c) Mean bout length (in seconds) plotted as mean across animals (coloured dots, representative of sleep states) and inter-state intervals for each state type (black bars). (d–f) Average firing rate per hour of putative inhibitory (pI)-cells shows significant differences across the day when analysing only data within each sleep/wake state. Individual hourly statistics are highlighted with symbols \wedge and \vee representing values above or below the mean, respectively, for each state. Means for each state are NREM = 5.106 Hz, REM = 7.012 Hz and wake = 5.446 Hz, each annotated in graph as coloured horizontal line (complete statistics in Table S1). As an effect of zeitgeber time (ZT), regardless of state, there is variability of pI-cell firing across time, $p < 0.001$, NREM (d), $p < 0.001$ for REM (e) and $p < 0.001$ for wake (f), one-way ANOVA. Graphs are box and whisker plots with line representing mean and with Tukey analysis. Outliers are shown as black dots. Background shows light/dark lighting. (g–i) Average firing rate per hour of putative excitatory (pE)-cells shows stable firing independent of both ZT and sleep-state. Graphs and statistics as shown same as in (d–f).

for NREM, REM and wake changes across 24 h (complete statistics in Table S1). During REM, pI-cells demonstrated significant increases from trough at ZT8–10 to ZT11–12, just before lights-off, suggesting anticipation of environmental change (Figure 2e, $p < 0.001$ for ZT8–10 compared with ZT11–12). pE-cell firing continued to show no modulation across the day within each sleep state (Figure 2g–i). Overall, this state-restricted analysis yielded comparable results to analysis without state restriction, demonstrating that state changes are not causing the spike rate modulations we observed.

3.3 | Sleep-associated hippocampal network oscillations peak during the light phase

Sleep and wake states are often defined by LFP oscillatory features such as NREM delta (0.1–3.9 Hz), REM theta (4–10 Hz) and waking theta (4–10 Hz). These oscillations play a role in coordinating neurons within each state and are critical for the hippocampus's role in information acquisition and consolidation (Girardeau & Lopes-Dos-Santos, 2021; Ognjanovski et al., 2017). Therefore, we next measured whether these sleep state-specific oscillations vary at different circadian times (Figure 3a,b). The power of the LFP band most characteristic of each state was divided by its mean power across the day and then averaged across animals for quantification (Figure 3c). NREM delta oscillations were found to be significantly higher during the light phase when sleep is more prominent in nocturnal mice (Figure 3c, top left, light blue). This is also true for another signature of NREM sleep in the hippocampus: sharp-wave ripples (SPWRs, Figure 3c, bottom right, dark blue). These power changes are also quantified and shown in the background of Figure 3d–f (coloured bars—* and blue line indicate difference between day and night in total NREM delta, $p < 0.001$). REM theta exhibits increases in the early part of the light phase and again in the middle of the dark phase (Figure 3c, top right, pink). In REM, we observed increases in theta power during the beginning of the light phase, with significant enrichment at ZT3–4 (Figure 3e, noted with *, $p = 0.003$ and $p = 0.008$, respectively, Holm–Sidak multiple comparison). Intriguingly, the mid-dark phase peaks (ZT18–22) of both NREM and REM sleep oscillation enrichments are coincident with reports showing mice often exhibit a ‘siesta’, or napping, period in the middle of the dark period (active phase) (Collins et al., 2020). Waking theta showed peaks in the middle of the dark phase (ZT19) the middle of the mouse's behaviourally active hours (Figure 3f, noted with *, $p < 0.007$, complete statistics for LFP in Table S2). These results

suggest that despite the presumed similarity of each episode of a given sleep state, LFPs in each state are modulated across 24 h.

Additionally, coupling between neuronal firing and LFP oscillations is a signature of specific sleep states (Ognjanovski et al., 2017; Watson et al., 2018). To measure communication between these, we measured SFC to the frequency bands described in NREM, REM and wake. We observe higher SFC of pE-cells compared with pI-cells across all oscillations (Figure 3d–f, black lines). During NREM, pE firing-delta coherence was enriched around light transitions (ZT1, 14 and 21–23, complete analysis in Table S3), intriguingly when delta power is lowest (Figure 3d, $p < 0.020$, delta is blue bars in background). Conversely, during REM, pE-cell coherence was highest at ZT19 ($p < 0.001$), in conjunction with enrichments in REM theta (Figure 3e, pink bars). During wake, pE- and pI-cell coherence both decrease at ZT13–14, in the initial stages in the mouse's ‘active’ period (Figure 3f, $p < 0.04$). This indicates that not only were the oscillations power-modulated as an effect of time, but so was the interaction of pI- and pE-cells with these rhythms.

3.4 | Electrophysiological background signatures as a behavioural baseline

We summarize our overall findings in what we collectively refer to as the EBS—in graphical format in Figure 4. Data from previous figures presented are shown here z-scored so they can be compared. These collective metrics are indicative of fluctuating baseline signals of animals that are unperturbed in their homecage. It is visually evident that both LFP and pI-cell firing vary across the 24-h cycle, and spike-field coupling shows some variance too. But in this display, the pE population behaviour is very apparent: strong consistency even in the face of variance all around. This combined display of multiple EBS metrics thus allows a clear picture of both dynamism (ultradian patterns in LFP) and invariance (static pE-cell firing) across a physiologic timescale, in this case across the 24-h day.

4 | DISCUSSION

Here we reveal the endogenous rhythms of in vivo hippocampal network activity in unperturbed mice across 24-h periods. We show that hippocampal electrophysiology has temporally structured dynamics in the absence of introduced stimuli or tasks. These new findings were made using an EBS approach emphasizing measurement of the long-term background and tone of the electrical network.

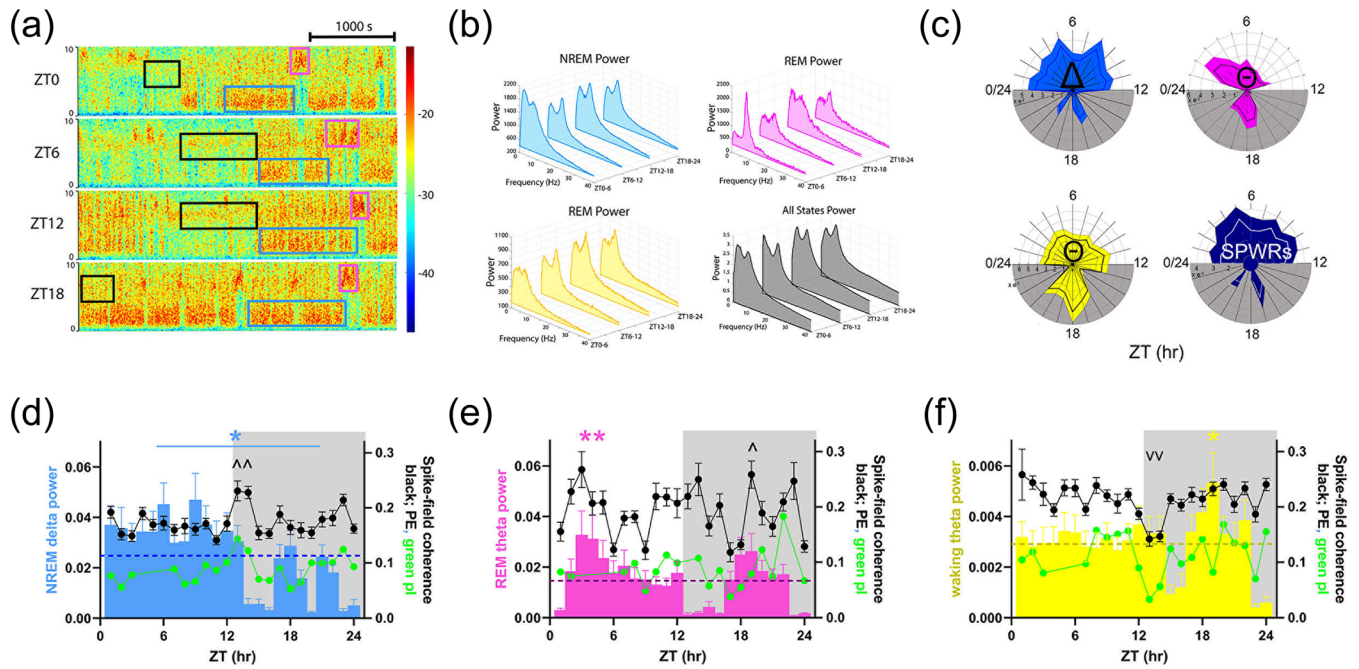


FIGURE 3 Oscillatory signatures of sleep states are differentially enriched across the day (a) Example 1-h spectrogram segments for frequencies 0–10 Hz at ZT0, 6, 12 and 18. Coloured boxes correspond to instances of non-rapid eye movement (NREM) delta (0.5–3.9 Hz, blue), rapid eye movement (REM) theta (4–10 Hz, pink) and waking theta (4–10 Hz, black). (b) Representative power spectral density graphs for representative animal within each state (NREM delta - blue, REM theta - pink, waking theta - yellow, total power - black) for the same zeitgeber times (ZTs) shown in (a). (c) Radial plots showing normalized power per hour within each state shown in colours corresponding to (b). Sharp-wave ripples (SPWRs - 150–250 Hz, dark blue) were also characterized. Each ring on plot corresponds to a value of $1e^{-2}$ (NREM and REM), $1e^{-3}$ (wake) and $1e^{-5}$ (NREM SPWRs) and each wedge represents an hour from ZT0/24. Darker line (white for SPWRs) is mean spectral power. (d–f) Spectral band power (coloured bars, same as in c, left axis) and spike-field coherence (spike-field coherence [SFC] - dots and lines, right axis) for putative excitatory (pE)-cells (black) and putative inhibitory (pI)-cells (green) within each state for each hour. Local field potential (LFP) power per hour within each state shown (coloured bars, left axis, normalized by within-state mean). Dashed lines (dark blue, deep pink, dark yellow) on each graph represent the mean daily LFP for the given frequency band. \wedge indicates statistical peaks and \vee statistical troughs in the SFC data, by multiple pairwise testing with Holm–Sidak correction. (d) NREM delta (blue bar and * above graph) indicate significant difference between delta power during the light phase (ZT1–12) and dark phase (ZT13–24), $p < 0.001$. All error bars are \pm SEM. NREM delta coherence at ZT14 significantly greater relative to ZT4–6, 13–14 and 21–24 $p < 0.02$. Complete statistics in Table S3. (e) Power and SFC as in (d) for REM theta (pink bars). $p < 0.001$ one-way ANOVA for time-of-day effects. Peak at ZT3–4, pairwise multiple comparison, $p < 0.05$, Holm–Sidak post-hoc test; pE-cell SFC significantly peaks at ZT19 relative to ZT9 and ZT17, $p < 0.001$. \wedge indicates increased compared with mean. (f) Power and SFC as in (d) for waking theta. Waking theta (yellow) $p < 0.001$ for ZT20–ZT24, $p = 0.002$ for ZT16–ZT20 and $p = 0.007$ for ZT17–ZT20, and SPWRs (dark blue) $p = 0.013$ for ZT1–12 versus ZT13–24. pE-cell SFC shows a statistical trough at ZT13–14, $p < 0.04$. Complete statistics are shown in Tables S2 and S3.

4.1 | pI- versus pE-cell firing across 24-h

One finding of particular interest in this data is the stability of the pE-cell population despite the 24-h variance in both pI-cell firing and oscillations. The remarkable stability of pE-cell firing despite such clear changes in the network environment suggests regulation of excitatory cells may be homeostatically maintained—perhaps due to the import of pE neurons in encoding and action control (Hengen et al., 2013). Of note, this stability is maintained whether analysed across sleep/wake states or within states.

Previous studies of hippocampal in vivo cell firing showed modulation by a sinusoid of period 25 h (Munn & Bilkey, 2012). However, these recordings were not continuous, with animals recording 20 min every hour, moving between recording chambers and showed much variation with a limited sample size. The continuous, freely-moving recordings presented here provide important direct evidence of naturally occurring neuronal patterns over the day.

In contrast to the pE population, our pI-cell population shows ultradian (<24 h) modulation around the clock with two prominent troughs in firing some hours

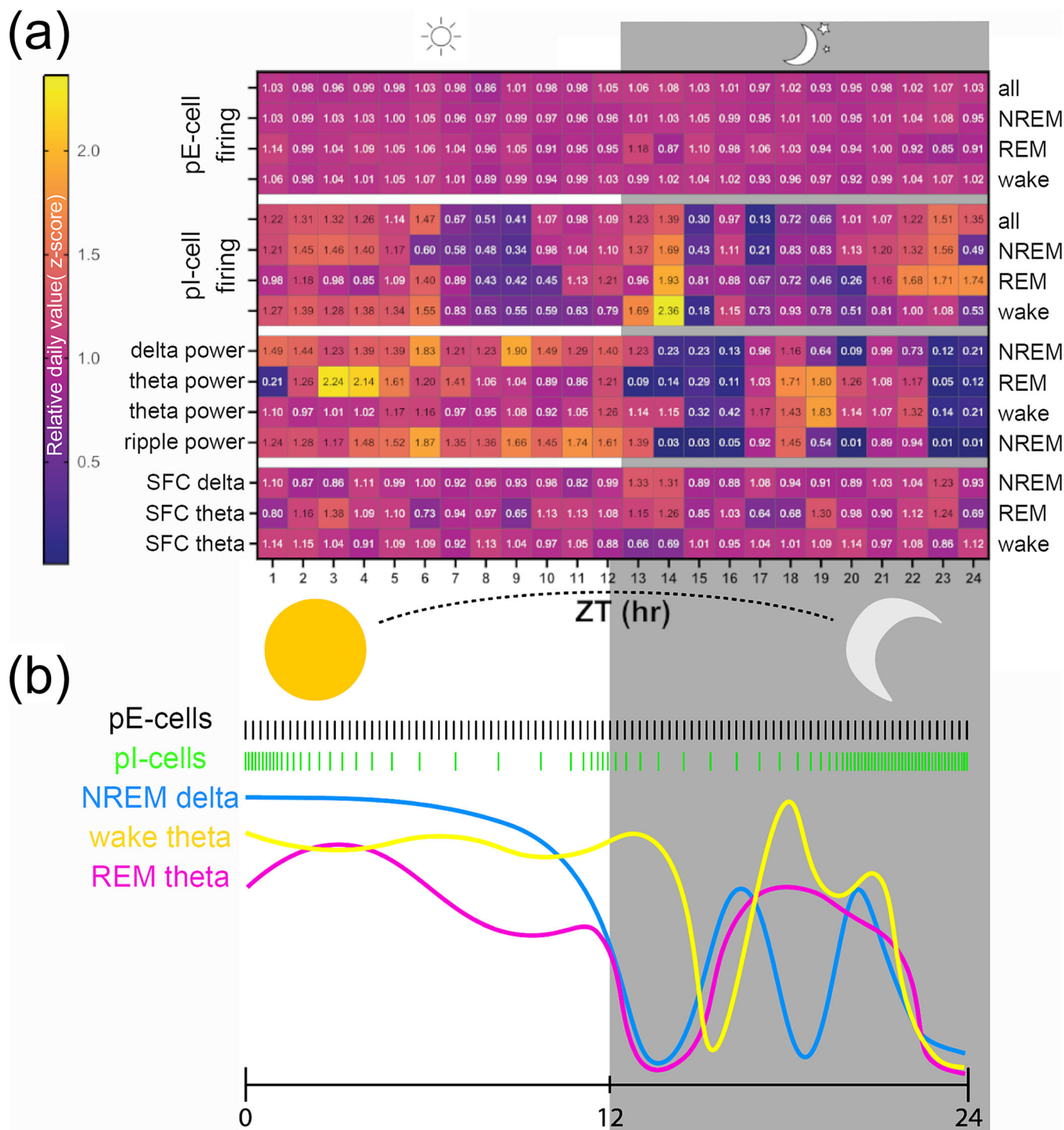


FIGURE 4 Summary of normalized time-of-day effects on different electrophysiological background signatures (EBSs). (a) Normalized values per each metric across the day are plotted in hour bins ($n = 10$ mice). Values are z-scores per each animal for each feature, averaged across all animals. Left labels denote type of EBS analysis: putative excitatory (pE)- and putative inhibitory (pI)-cell firing rates, local field potential (LFP) powers and spike-field coherence (SFC). Sleep states labelled at right are shown as individual rows. Evident is pE stability (top rows) which contrasts with pI-cell variance that includes peaks around zeitgeber time (ZT) hours 24/0 and troughs around hours 9 and 14–15 across all sleep states. For LFP level changes, non-rapid eye movement (NREM) and rapid eye movement (REM) sleep generally show light-hours (inactive time) enrichment of oscillatory power, with secondary peak around ZT18, in the middle of the animals' active period. Waking theta remains elevated across the light period, before dropping after lights off, but also shows peak at ZT19. (b) Visual depiction of the z-scores presented in (a). The pE- and pI-cell firing rates are shown graphically in black and green, respectively. The continuous LFP are shown with blue, yellow and pink coloured lines for NREM-delta and REM and wake theta, respectively, as shown in Figure 3.

before and some hours after the light-to-dark transition. Again, these pI-specific dynamics occur whether or not sleep/wake states are used to confine data. These inhibitory dynamics may be expected because inhibitory cells are known to be more strongly linked to neuromodulatory systems than excitatory cells (Kepecs & Fishell, 2014; Lee et al., 2010; Rudy et al., 2011; Wester & McBain, 2014). This feature may render inhibitory cells particularly responsive to a changing environmental context, such as occurring around the 24-h clock (Avery & Krichmar, 2017). Indeed, hippocampal interneuron modulation has been shown to expand dynamic range, aid pattern separation and enable phase processing in sensory responses (Ahnaou et al., 2017; Chamberland & Topolnik, 2012; Kann et al., 2014; Varga et al., 2012).

Our recorded population could include several subtypes of hippocampal GABAergic interneurons (Klausberger & Somogyi, 2008), but is likely to be predominantly composed of parvalbumin (PV)-positive cells based on the waveform-based selection we used (Hu et al., 2014; Stark et al., 2013). Previous reports show the necessity and sufficiency of PV-interneurons in learning, as manipulations of these cells' roles in memory in the beginning of the light period resulted in loss of theta rhythms and spontaneously occurring hippocampal ripples (Ognjanovski et al., 2017; Roach et al., 2018; Stark et al., 2014). The beginning of the light period is the time at which we show naturally occurring enrichments in sleep-specific oscillations and pI-cell firing. Furthermore, the hours-timescale rhythmicity observed in pI-cell population rates may be reflective of LFP involvement in hippocampal functionality at different circadian times.

4.2 | Sleep LFPs and timing of sleep

Relatedly, we observe that delta oscillatory power was higher during the day (normal inactivity hours) than the night—even within NREM. This could imply that sleep is deepened during the animal's evolutionarily conserved sleep time (days in mice)—compared with opposite-phase NREM bouts. Complimentarily, the elevated waking theta observed across the dark (active) period suggests that awake attention may be greater during the typical wake phase. This points to a phenomenon of potentiation of 'more wakeful wake' during the night and 'more restful sleep' in the day for these nocturnal animals. Such synchronization between time of day and oscillatory tendencies may have benefits because desynchrony between light cycles and brain state cycles—such as those observed in shift work—can worsen neuropsychiatric disorders, suggesting that sleep and circadian patterns should be aligned in the healthy state

(Kyriacou & Hastings, 2010; Walker et al., 2020). In fact, one human study shows sleep state-independent modulation of spectral power, suggesting this finding may be relatively general (Gundel & Hilbig, 1983). This work corroborates our findings in mice, suggesting the universality of this effect.

Interestingly, we find that REM sleep shows an intermediate phenotype with the power of theta oscillations increased during the beginning of the day as well as the middle of the night. In fact, we observe during REM that pE-cell SFC increases in coordination with theta power, possibly due to acetylcholine-dynamics, which are generally up-modulated during active network engagement (Minces et al., 2017; Vandecasteele et al., 2014). This suggests that the time scales of molecular, cellular and network-wide activity pattern modulation vary as a function of behavioural state. Alternatively, REM theta power peaks during the dark period could be occurring within 'siesta' periods reported in mouse circadian studies (Collins et al., 2020) and thought to be important in longer-term roles the hippocampus plays in the context of memory formation.

Akin to our observations in CA1 pI-cell firing rates, previous circadian clock gene work in the dentate gyrus (DG) region of the hippocampus has shown that core-clock gene, *per2*, expression has a bimodal distribution of peaks at light transitions (Curie et al., 2015). Because CA1 receives inputs from DG, these pI-cells may be processing environmental changes to support pyramidal cell firing at the molecular level. This may be of import given the role of DG in novelty detection, which is important in learning (Hunsaker et al., 2008). Therefore, our analysis of the daily rhythms of LFP power both aligns with previous behavioural and molecular learning and also provides a specific quantifiable in vivo biomarker of circadian potential for timing of learning.

4.3 | Divergent modulation of various EBS measures across 24-h

While LFP band powers, spike-field coupling and pI-cell population firing rates show modulation by time of day, pE-neurons show consistent firing in each hourly time bin. It may be that pE-cells, as the primary mediators of perception and motor output, are maintained at constant population activity rates in healthy animals to provide reliable sensorimotor interaction with the environment. The remarkable stability of the mean activity of this population implies that pE-cells may be homeostatically managed. Of note, this stability is in relation to the population and at an hourly timescale, so there is no implication here that excitatory neurons are unresponsive to

stimuli. In fact, we know that is not true at shorter time-scales and with specific experiences (O'Keefe, 1976, 1979). An interpretation of the contrast between pE- and pI-cell 24-h rhythms is that the pI-cell variation may be a compensatory mechanism to enable homeostatic management of pE-cell firing rate.

The mechanisms of this maintenance of firing despite fluctuation in LFP and pI rates need to be explored, but pI- neurons, or particular sub-populations of inhibitory cells, may modulate pE populations to broadly maintain stability in compensation for changes in oscillations, neuromodulators and other factors. For example, it is known that parvalbumin (PV)-positive interneurons, can feedback inhibit pyramidal populations if pyramidal firing rates increase too much, preventing epilepsy (Trevelyan et al., 2006). Similar mechanisms may be at work to maintain consistent function through the day. We have certainly not measured all factors potentially controlling pE rates, and so the picture here, while novel, is incomplete.

Time-of-day modulation of LFP power may be created by alterations in neuromodulator tone around the clock or by alterations in responsiveness to those modulators around the clock (Korshunov et al., 2017; Mochizuki et al., 1992; Pontes et al., 2010; Trevelyan, 2009). The impacts and mechanisms of this are not yet known.

4.4 | Limitations and directions for future research

The results presented here have the limitation of being from a single, 24-h cycle per animal because they were funded via a European Union grant with an emphasis on reduction of animals used. As a result, this data were originally recorded as part of data sets for papers Ognjanovski et al., 2014, 2017 using the 24-h recordings either prior to learning or behavioural paradigms or in animals who did not undergo any learning or behavioural paradigms. We were thus able to revisit this data using an EBS approach to time-of-day effects rather than the original learning-oriented questions intended for these recordings.

We are excited about the EBS approach because it allows us to add dozens of metrics over time with the goal of approaching network states as constantly evolving. In the future, we plan to add more measures to EBS to more completely quantify the network's overall state. Measures will include assembly activity strength, functional coupling of pairs of neurons in E-E, I-I, E-I and I-E pairs of neurons, power spectral slope, burst ratio, synchrony, infra-slow power, firing rate distribution width and many others generated from both theory and observation. This is our first EBS-oriented paper we have published, and

future efforts with purpose-designed experiments will have yet richer background network characterizations.

We note that the behaviour of these cohorts of C57Bl6J mice is 'atypical' for an idealized nocturnal species. However, there is clearly a modulation of sleep bouts and inter-bout intervals by time of day with somewhat more sleep in the day, as well as shorter times between bouts (see Figure S1). Second, the observed pattern shows crepuscular-like effects in this strain, and indeed, much literature recently is pointing out the inbreeding and constant conditions of laboratory settings show mice having more crepuscular behaviour. Possibly relatedly, in other species, the spectrum of light used in most laboratories was found to induce crepuscular rhythms, whereas fuller-spectrum light led to less crepuscular modulation (Kim et al., 2023). Third, our sleep data is shown openly, and despite this modulation of sleep state throughout the 24-h cycle, it does not modulate the LFP and spiking data. Indeed, LFP shows a strong modulation by circadian light pattern. And in other analyses, spiking patterns are modulated by time of day, despite analyses within a given sleep state. Therefore, we show that time of day rather than sleep state predicts LFP and spiking.

Furthermore, as the original data set was only males, we are limited in our conclusions but acknowledge sex differences between males and females (An et al., 2011; Tsao et al., 2023). Lastly, the number of pI cells and the ratio of pE:pI cells within each animal varied, with some animals having no pI cells noted in our hippocampal pyramidal layer recordings. This may limit some interpretations of pI findings, although we are not aware of particular directions in which this would bias our findings. Further analysis with updated recording techniques could address this.

Future experiments could thus include recoding of (1) a broader range of hippocampal laminar electrode placements, (2) multiple repeated 24-h cycles to address theoretical sampling problems (though we are not aware of any explicit problems here) and (3) experiments on females including estrous cycle monitoring because estrous phase modulates hippocampal structure and physiology (Kundakovic & Rocks, 2022; Scharfman et al., 2003).

Despite our limitations, this approach has provided valuable new insights. In particular, as framed in Figure 4, our EBS approach shows general time-of-day trends across C57Bl6 mice given the common 12:12 environmental cycles used by many labs and often do not note in published studies. Considerations of such background dynamics are likely to benefit future work, considering that we show they impact network function. Deepening future experiments will only improve that understanding.

4.5 | Conclusions

Because electrophysiology is the means by which neural network structure and molecular state are translated into perception, behaviour and cognition, we undertook an approach of long-term baseline measurement of the electrophysiologic network: the EBS approach. This manner of quantification can link molecular and structural studies with network and behavioural findings because it has the timescale to overlap with molecular and structural methods but measures online network function.

Future work can focus on whether the findings here are maintained in pathological or stress states, possibly including those with abnormal circadian cycles. This includes conditions that induce cognitive and mental problems in humans, such as 'shiftwork' schedules or chronic sleep deprivation. This can provide new network function-level biomarkers or mechanistic insights into pathological states.

Overall, our work quantifies, in vivo, natural variations in hippocampal network activity in freely behaving animals. We show that excitatory neuron populations fire stably at hours timescale despite changing sleep states, spike-field coupling and interneuron population activity. This data, demonstrating the contrast between excitatory and inhibitory population activity and local oscillatory dynamics, provides important new data about healthy network function around the 24-h cycles that control daily behaviour and cognition patterns.

AUTHOR CONTRIBUTIONS

Idea conceptualization and methodology was done by Nicolette Ognjanovski. Initial investigation was done by Nicolette Ognjanovski, Emma Charlett-Green and Sofie van Koppen, with further data curation done by David S. Kim, Emma Charlett-Green and Sofie van Koppen. Funding acquisition was provided by Nicolette Ognjanovski, Sara J. Aton and Brendon O. Watson. Software and programming were done by David S. Kim and Ethan Goldiez. Visualization of the figures for this paper was accomplished by David S. Kim, Ethan Goldiez and Sofie van Koppen. The writing of the original draft was done by Nicolette Ognjanovski and Brendon O. Watson, with assistance from Sara J. Aton. Reviewing and editing of the draft were done by Nicolette Ognjanovski, Ethan Goldiez and Brendon O. Watson. All project administration was done by Nicolette Ognjanovski.

ACKNOWLEDGEMENTS

This work was supported by the NIH (MH107662), the Pritzker Neuropsychiatric Research Consortium, the A. Alfred Taubman Medical Research Institute, the Eisenberg Depression Center and the University of

Michigan Neuroscience Scholars fund to BOW. Additional funding from the Michigan Medicine Sleep Disorders Center: Gilmore Sleep Fellowship and Marie Curie Horizons 2020 Leading Fellowship (no. 707404) to NO provided while at the Leiden University Medical Center.

CONFLICT OF INTEREST STATEMENT

The authors of this paper have no conflicts of interest to declare.

PEER REVIEW

The peer review history for this article is available at <https://www.webofscience.com/api/gateway/wos/peer-review/10.1111/ejn.16619>.

DATA AVAILABILITY STATEMENT

The data that support the findings of this study are openly available via the University of Michigan DataDen at <https://arc.umich.edu/data-den/>. Collection:347 <https://app.globus.org/file-manager/collections> Path:/umms-brendonw/HippoCircadian/. Additionally, derived data of this study are available from the corresponding author [NO] on request.

ORCID

Nicolette Ognjanovski  <https://orcid.org/0000-0002-0807-7526>

REFERENCES

- Ahnaou, A., Moechars, D., Raeymaekers, L., Biermans, R., Manyakov, N. V., Böttelbergs, A., Wintolders, C., Van Kolen, K., Van De Castele, T., Kemp, J. A., & Drinkenburg, W. H. (2017). Emergence of early alterations in network oscillations and functional connectivity in a tau seeding mouse model of Alzheimer's disease pathology. *Scientific Reports*, 7, 14189. <https://doi.org/10.1038/s41598-017-13839-6>
- An, X.-L., Zou, J.-X., Wu, R.-Y., Yang, Y., Tai, F.-D., Zeng, S.-Y., Jia, R., Zhang, X., Liu, E.-Q., & Broders, H. (2011). Strain and sex differences in anxiety-like and social behaviors in C57BL/6J and BALB/cJ mice. *Experimental Animals*, 60, 111–123. <https://doi.org/10.1538/expanim.60.111>
- Avery, M. C., & Krichmar, J. L. (2017). Neuromodulatory systems and their interactions: A review of models, theories, and experiments. *Frontiers in Neural Circuits*, 11, 1–18. <https://doi.org/10.3389/fncir.2017.00108>
- Brecht, M., Schneider, M., Sakmann, B., & Margrie, T. (2003). Movements evoked by intracellular stimulation of single pyramidal cells in layer 5 and 6 of rat motor cortex. *Nature*, 427, 704–710. <https://doi.org/10.1038/nature02266>
- Bridi, M. C. D., Zong, F. J., Min, X., Luo, N., Tran, T., Qiu, J., Severin, D., Zhang, X. T., Wang, G., Zhu, Z. J., He, K. W., & Kirkwood, A. (2020). Daily oscillation of the excitation-inhibition balance in visual cortical circuits. *Neuron*, 105, 621–629.e4. <https://doi.org/10.1016/j.neuron.2019.11.011>
- Brown, T. M., & Piggins, H. D. (2009). Spatiotemporal heterogeneity in the electrical activity of suprachiasmatic nuclei neurons and

- their response to photoperiod. *Journal of Biological Rhythms*, 24, 44–54. <https://doi.org/10.1177/0748730408327918>
- Chamberland, S., & Topolnik, L. (2012). Inhibitory control of hippocampal inhibitory neurons. *Frontiers in Neuroscience*, 6, 165. <https://doi.org/10.3389/fnins.2012.00165>
- Collins, B., Pierre-Ferrer, S., Muheim, C., Lukacsovich, D., Cai, Y., Spinnler, A., Herrera, C. G., Wen, S. A., Winterer, J., Belle, M. D. C., Piggins, H. D., Hastings, M., Loudon, A., Yan, J., Földy, C., Adamantidis, A., & Brown, S. A. (2020). Circadian VIPergic neurons of the suprachiasmatic nuclei sculpt the sleep-wake cycle. *Neuron*, 108, 486–499.e5. <https://doi.org/10.1016/j.neuron.2020.08.001>
- Curie, T., Maret, S., Emmenegger, Y., & Franken, P. (2015). In vivo imaging of the central and peripheral effects of sleep deprivation and suprachiasmatic nuclei lesion on PERIOD-2 protein in mice. *Sleep*, 38, 1381–1394. <https://doi.org/10.5665/sleep.4974>
- Delgado, J. M. R. (1952). Responses evoked in waking cat by electrical stimulation of motor cortex. *The American Journal of Physiology*, 171, 436–446. <https://doi.org/10.1152/ajplegacy.1952.171.2.436>
- Eckel-Mahan, K. L. (2012). Circadian oscillations within the hippocampus support memory formation and persistence. *Frontiers in Molecular Neuroscience*, 5, 1–4. <https://doi.org/10.3389/fnmol.2012.00046>
- Frank, M. G. (2021). Renormalizing synapses in sleep: The clock is ticking. *Biochemical Pharmacology*, 191, 114533. <https://doi.org/10.1016/j.bcp.2021.114533>
- Girardeau, G., & Lopes-Dos-Santos, V. (2021). Brain neural patterns and the memory function of sleep. *Science*, 374, 560–564. <https://doi.org/10.1126/science.abi8370>
- Gundel, A., & Hilbig, A. (1983). Circadian acrophases of powers and frequencies in the waking EEG. *The International Journal of Neuroscience*, 22, 125–133. <https://doi.org/10.3109/00207459308987391>
- Hengen, K. B., Lambo, M. E., VanHooser, S. D., Katz, D. B., & Turrigiano, G. G. (2013). Firing rate homeostasis in visual cortex of freely behaving rodents. *Neuron*, 80, 335–342. <https://doi.org/10.1016/j.neuron.2013.08.038>
- Houben, T., Deboer, T., Van Oosterhout, F., & Meijer, J. H. (2009). Correlation with behavioral activity and rest implies circadian regulation by SCN neuronal activity levels. *Journal of Biological Rhythms*, 24, 477–487. <https://doi.org/10.1177/0748730409349895>
- Hu, H., Gan, J., & Jonas, P. (2014). Fast-spiking, parvalbumin + GABAergic interneurons: From cellular design to microcircuit function. *Science*, 345, 1255263. <https://doi.org/10.1126/science.1255263>
- Hunsaker, M. R., Rosenberg, J. S., & Kesner, R. P. (2008). The role of the dentate gyrus, CA3a,b, and CA3c for detecting spatial and environmental novelty. *Hippocampus*, 18, 1064–1073. <https://doi.org/10.1002/hipo.20464>
- Jilg, A., Lesny, S., Peruzki, N., Schwegler, H., Selbach, O., Dehghani, F., & Stehle, J. H. (2010). Temporal dynamics of mouse hippocampal clock gene expression support memory processing. *Hippocampus*, 20, 377–388. <https://doi.org/10.1002/hipo.20637>
- Kann, O., Papageorgiou, I. E., & Draguhn, A. (2014). Highly energized inhibitory interneurons are a central element for information processing in cortical networks. *Journal of Cerebral Blood Flow & Metabolism*, 34, 1270–1282. <https://doi.org/10.1038/jcbfm.2014.104>
- Kepecs, A., & Fishell, G. (2014). Interneuron cell types are fit to function. *Nature*, 505, 318–326. <https://doi.org/10.1038/nature12983>
- Kim, A. B., Beaver, E. M., Collins, S. G., Kriegsfeld, L. J., Lockley, S. W., Wong, K. Y., & Yan, L. (2023). S-cone photoreceptors regulate daily rhythms and light-induced arousal/wakefulness in diurnal grass rats (*Arvicanthis niloticus*). *Journal of Biological Rhythms*, 38, 366–378. <https://doi.org/10.1177/07487304231170068>
- Klausberger, T., & Somogyi, P. (2008). Neuronal diversity and temporal dynamics: The unity of hippocampal circuit operations. *Science*, 321, 53–57. <https://doi.org/10.1126/science.1149381>
- Korshunov, K. S., Blakemore, L. J., & Trombley, P. Q. (2017). Dopamine: A modulator of circadian rhythms in the central nervous system. *Frontiers in Cellular Neuroscience*, 11, 91. <https://doi.org/10.3389/fncel.2017.00091>
- Kundakovic, M., & Rocks, D. (2022). Sex hormone fluctuation and increased female risk for depression and anxiety disorders: From clinical evidence to molecular mechanisms. *Frontiers in Neuroendocrinology*, 66, 101010. <https://doi.org/10.1016/j.yfrne.2022.101010>
- Kyriacou, C. P., & Hastings, M. H. (2010). Circadian clocks: Genes, sleep, and cognition. *Trends in Cognitive Sciences*, 14, 259–267. <https://doi.org/10.1016/j.tics.2010.03.007>
- Lee, S. H., Hjerling-Leffler, J., Zagha, E., Fishell, G., & Rudy, B. (2010). The largest group of superficial neocortical GABAergic interneurons expresses ionotropic serotonin receptors. *The Journal of Neuroscience*, 30, 16796–16808. <https://doi.org/10.1523/JNEUROSCI.1869-10.2010>
- Mariscal, P., Bravo, L., Llorca-Torrallba, M., Razquin, J., Miguelez, C., Suárez-Pereira, I., & Berrocoso, E. (2023). Sexual differences in locus coeruleus neurons and related behavior in C57BL/6J mice. *Biology of Sex Differences*, 14, 64. <https://doi.org/10.1186/s13293-023-00550-7>
- Maurer, A. P., & Nadel, L. (2021). The continuity of context: A role for the hippocampus. *Trends in Cognitive Sciences*, 25, 187–199. <https://doi.org/10.1016/j.tics.2020.12.007>
- Minces, V., Pinto, L., Dan, Y., & Chiba, A. A. (2017). Cholinergic shaping of neural correlations. *Proceedings of the National Academy of Sciences of the United States of America*, 114, 5725–5730. <https://doi.org/10.1073/pnas.1621493114>
- Miyawaki, H., & Diba, K. (2016). Regulation of hippocampal firing by network oscillations during sleep. *Current Biology*, 26(7), 893–902.
- Mochizuki, T., Yamatodani, A., Okakura, K., Horii, A., Inagaki, N., & Wada, H. (1992). Circadian rhythm of histamine release from the hypothalamus of freely moving rats. *Physiology & Behavior*, 51, 391–394. [https://doi.org/10.1016/0031-9384\(92\)90157-W](https://doi.org/10.1016/0031-9384(92)90157-W)
- Munn, R. G. K., & Bilkey, D. K. (2012). The firing rate of hippocampal CA1 place cells is modulated with a circadian period. *Hippocampus*, 22, 1325–1337. <https://doi.org/10.1002/hipo.20969>
- Nelson, W., Tong, Y. L., Lee, J. K., & Halberg, F. (1979). Methods for cosinor-rhythmometry. *Chronobiologia*, 6, 305–323.
- Ognjanovski, N., Maruyama, D., Lashner, N., Zochowski, M., & Aton, S. J. (2014). CA1 hippocampal network activity changes

- during sleep-dependent memory consolidation. *Frontiers in Systems Neuroscience*, 8, 61. <https://doi.org/10.3389/fnsys.2014.00061>
- Ognjanovski, N., Schaeffer, S., Wu, J., Mofakham, S., Maruyama, D., Zochowski, M., & Aton, S. J. (2017). Parvalbumin-expressing interneurons coordinate hippocampal network dynamics required for memory consolidation. *Nature Communications*, 8, 15039. <https://doi.org/10.1038/ncomms15039>
- O'Keefe, J. (1976). Place units in the hippocampus of the freely moving rat. *Experimental Neurology*, 51, 78–109. [https://doi.org/10.1016/0014-4886\(76\)90055-8](https://doi.org/10.1016/0014-4886(76)90055-8)
- O'Keefe, J. (1979). A review of the hippocampal place cells. *Progress in Neurobiology*, 13, 419–439. [https://doi.org/10.1016/0301-0082\(79\)90005-4](https://doi.org/10.1016/0301-0082(79)90005-4)
- Oliva, A., Fernández-Ruiz, A., Leroy, F., & Siegelbaum, S. A. (2020). Hippocampal CA2 sharp-wave ripples reactivate and promote social memory. *Nature*, 587, 264–269. <https://doi.org/10.1038/s41586-020-2758-y>
- Paul, J. R., Davis, J. A., Goode, L. K., Becker, B. K., Fusilier, A., Meador-Woodruff, A., & Gamble, K. L. (2020). Circadian regulation of membrane physiology in neural oscillators throughout the brain. *The European Journal of Neuroscience*, 51, 109–138. <https://doi.org/10.1111/ejn.14343>
- Pontes, A. L. B. D., Engelberth, R. C. G. J., Nascimento, E. D. S., Cavalcante, J. C., Costa, M. S. M. D. O., Pinato, L., Toledo, C. A. B. D., & Cavalcante, J. D. S. (2010). Serotonin and circadian rhythms. *Psychology & Neuroscience*, 3, 217–228. <https://doi.org/10.3922/j.pns.2010.2.011>
- Ramkisoensing, A., & Meijer, J. H. (2015). Synchronization of biological clock neurons by light and peripheral feedback systems promotes circadian rhythms and health. *Frontiers in Neurology*, 6, 128. <https://doi.org/10.3389/fneur.2015.00128>
- Rawashdeh, O., Parsons, R., & Maronde, E. (2018). Clocking in time to gate memory processes: The circadian clock is part of the ins and outs of memory. *Neural Plasticity*, 2018, 6238989. <https://doi.org/10.1155/2018/6238989>
- Roach, J. P., Pidde, A., Katz, E., Wu, J., Ognjanovski, N., Aton, S. J., & Zochowski, M. R. (2018). Resonance with sub-threshold oscillatory drive organizes activity and optimizes learning in neural networks. *Proceedings of the National Academy of Sciences*, 115, E3017–E3025. <https://doi.org/10.1073/pnas.1716933115>
- Rudy, B., Fishell, G., Lee, S. H., & Hjerling-Leffler, J. (2011). Three groups of interneurons account for nearly 100% of neocortical GABAergic neurons. *Developmental Neurobiology*, 71, 45–61. <https://doi.org/10.1002/dneu.20853>
- Russell, G., & Lightman, S. (2019). The human stress response. *Nature Reviews. Endocrinology*, 15, 525–534. <https://doi.org/10.1038/s41574-019-0228-0>
- Schaap, J., Albus, H., VanderLeest, H. T., Eilers, P. H. C., Détári, L., & Meijer, J. H. (2003). Heterogeneity of rhythmic suprachiasmatic nucleus neurons: Implications for circadian waveform and photoperiodic encoding. *Proceedings of the National Academy of Sciences of the United States of America*, 100, 15994–15999. <https://doi.org/10.1073/pnas.2436298100>
- Scharfman, H. E., Sollas, A. L., Berger, R. E., & Goodman, J. H. (2003). Electrophysiological evidence of monosynaptic excitatory transmission between granule cells after seizure-induced mossy fiber sprouting. *Journal of Neurophysiology*, 90, 2536–2547. <https://doi.org/10.1152/jn.00251.2003>
- Skilling, Q. M., Eniwaye, B., Clawson, B. C., Shaver, J., Ognjanovski, N., Aton, S. J., & Zochowski, M. (2021). Acetylcholine-gated current translates wake neuronal firing rate information into a spike timing-based code in non-REM sleep, stabilizing neural network dynamics during memory consolidation. *PLoS Computational Biology*, 17, e1009424. <https://doi.org/10.1371/journal.pcbi.1009424>
- Stark, E., Eichler, R., Roux, L., Fujisawa, S., Rotstein, H. G., & Buzsáki, G. (2013). Inhibition-induced theta resonance in cortical circuits. *Neuron*, 80, 1263–1276. <https://doi.org/10.1016/j.neuron.2013.09.033>
- Stark, E., Roux, L., Eichler, R., Senzai, Y., Royer, S., & Buzsáki, G. (2014). Pyramidal cell-interneuron interactions underlie hippocampal ripple oscillations. *Neuron*, 83, 467–480. <https://doi.org/10.1016/j.neuron.2014.06.023>
- Terranova, J. I., Yokose, J., Osanai, H., Marks, W. D., Yamamoto, J., Ogawa, S. K., & Kitamura, T. (2022). Hippocampal-amygdala memory circuits govern experience-dependent observational fear. *Neuron*, 110, 1416–1431.e13. <https://doi.org/10.1016/j.neuron.2022.01.019>
- Thomas, C. W., Guillaumin, M. C. C., McKillop, L. E., Achermann, P., & Vyazovskiy, V. V. (2020). Global sleep homeostasis reflects temporally and spatially integrated local cortical neuronal activity. *eLife*, 9, e54148. <https://doi.org/10.7554/eLife.54148>
- Trevelyan, A. J. (2009). The direct relationship between inhibitory currents and local field potentials. *The Journal of Neuroscience*, 29, 15299–15307. <https://doi.org/10.1523/JNEUROSCI.2019-09.2009>
- Trevelyan, A. J., Sussillo, D., Watson, B. O., & Yuste, R. (2006). Modular propagation of epileptiform activity: Evidence for an inhibitory veto in neocortex. *The Journal of Neuroscience*, 26, 12447–12455. <https://doi.org/10.1523/JNEUROSCI.2787-06.2006>
- Tsao, C.-H., Wu, K.-Y., Su, N. C., Edwards, A., & Huang, G. J. (2023). The influence of sex difference on behavior and adult hippocampal neurogenesis in C57BL/6 mice. *Scientific Reports*, 13, 17297.
- van Oosterhout, F., Lucassen, E. A., Houben, T., vanderLeest, H., Antle, M., & Meijer, J. (2012). Amplitude of the SCN clock enhanced by the behavioral activity rhythm. *PLoS ONE*, 7, e39693. <https://doi.org/10.1371/journal.pone.0039693>
- Vandecasteele, M., Varga, V., Berényi, A., Papp, E., Barthó, P., Venance, L., Freund, T. F., & Buzsáki, G. (2014). Optogenetic activation of septal cholinergic neurons suppresses sharp wave ripples and enhances theta oscillations in the hippocampus. *Proceedings of the National Academy of Sciences of the United States of America*, 111, 13535–13540. <https://doi.org/10.1073/pnas.1411233111>
- Varga, C., Golshani, P., & Soltesz, I. (2012). Frequency-invariant temporal ordering of interneuronal discharges during hippocampal oscillations in awake mice. *Proceedings of the National Academy of Sciences*, 109, E2726–E2734.
- Walker, W. H., Walton, J. C., DeVries, A. C., & Nelson, R. J. (2020). Circadian rhythm disruption and mental health. *Translational Psychiatry*, 10, 28. <https://doi.org/10.1038/s41398-020-0694-0>

- Watson, B. O., Ding, M., & Buzsáki, G. (2018). Temporal coupling of field potentials and action potentials in the neocortex. *The European Journal of Neuroscience*, *48*, 2482–2497. <https://doi.org/10.1111/ejn.13807>
- Watson, B. O., Levenstein, D., Greene, J. P., Gelineau, J. N., & Buzsáki, G. (2016). Network homeostasis and state dynamics of neocortical sleep. *Neuron*, *90*, 839–852. <https://doi.org/10.1016/j.neuron.2016.03.036>
- Wester, J. C., & McBain, C. J. (2014). Behavioral state-dependent modulation of distinct interneuron subtypes and consequences for circuit function. *Current Opinion in Neurobiology*, *29*, 118–125. <https://doi.org/10.1016/j.conb.2014.07.007>

SUPPORTING INFORMATION

Additional supporting information can be found online in the Supporting Information section at the end of this article.

How to cite this article: Ognjanovski, N., Kim, D. S., Charlett-Green, E., Goldiez, E., van Koppen, S., Aton, S. J., & Watson, B. O. (2025). Daily rhythms drive dynamism in sleep, oscillations and interneuron firing, while excitatory firing remains stable across 24 h. *European Journal of Neuroscience*, *61*(1), e16619. <https://doi.org/10.1111/ejn.16619>